Available online at www.sciencedirect.com
SCIENCE DIRECT®
International Journal of Solids and Structures 42 (2005) 4795–4810
INTERNATIONAL JOURNAL OF SOLIDS and STRUCTURES
www.elsevier.com/locate/ijsolstr

Vapor pressure and residual stress effects on failure of an adhesive film

H.B. Chew, T.F. Guo, L. Cheng *

Department of Mechanical Engineering, National University of Singapore, Blk EA, 9 Engineering Drive 1, Singapore 117576, Singapore

Received 2 March 2004; received in revised form 17 January 2005
Available online 23 February 2005

Abstract

Surface-mount plastic encapsulated microcircuits (PEM) are susceptible to temperature- and moisture-induced failures during reflow soldering. Adhesive failures in PEMs are studied using a model problem of a ductile adhesive joining two elastic substrates. The polymeric adhesive contains a centerline crack. The adhesive film is stressed by remote loading and residual stresses. Voids in the adhesive are pressurized by rapidly expanding water vapor. The computational study addresses three competing failure mechanisms: (i) extended contiguous damage zone emanating from the crack; (ii) multiple damage zones forming at distances of several film thicknesses ahead of the crack; and (iii) extensive damage developing along film–substrate interfaces. The second failure mechanism is found in low porosity adhesives, while the first is dominant in high porosity adhesives. The first is also the likely failure mode when voids in the adhesive are subjected to high vapor pressure. The third damage mechanism is operative in low porosity adhesives subjected to high residual stress. In general, both residual stress and vapor pressure exert pronounced effects on failure modes. Vapor pressure, in particular, accelerates voiding activity and growth of the damage zone offering insights into the catastrophic nature of popcorn cracking.

Keywords: Fracture mechanisms; Porous material; Void growth; Damage; Adhesive; Polymers

1. Introduction

Surface-mount plastic encapsulated microcircuits (PEM) are susceptible to several types of temperature- and moisture-induced interface delamination and package cracking during the reflow soldering process. This vulnerability arises from the hygroscopic nature of polymeric molding compounds and adhesives used

* Corresponding author. Tel.: +65 6874 6888; fax: +65 6779 1459.
E-mail address: mpecl@nus.edu.sg (L. Cheng).

0020-7683/$ - see front matter © 2005 Elsevier Ltd. All rights reserved.
doi:10.1016/j.ijsolstr.2005.01.012

in fabricating PEMs. When these plastic packages encounter a humid environment, moisture is absorbed into pores and cavities of polymeric materials as well as polymer/die interfaces. During reflow soldering, the entire plastic package is heated to temperatures as high as 220–260 °C. These temperatures exceed the glass transition temperatures, T_g, of the adhesives and molding compounds. At such temperatures, the absorbed moisture rapidly vaporizes into steam, raising vapor pressure to levels comparable to the yield stress of adhesives and molding compounds. At the same time, the mismatches between the coefficients of thermal expansion (CTE) for die/adhesive and die/molding compound interfaces are also greater when the package temperature exceeds the respective T_gs. The high vapor pressures and thermal stresses noted above are imposed on adhesives and molding compounds which had experienced significant loss of mechanical strength (related to T_g effects). This scenario presents one particular set of conditions under which the voids grow rapidly leading to film rupture and interface delamination. When the crack reaches the package exterior, the high-pressure water vapor is suddenly released, producing an audible pop sound. This mechanism of failure is termed as popcorn cracking (Fukuzawa et al., 1985).

Three distinct types of temperature- and moisture-induced popcorn cracking have been reported for PEMs (Omi et al., 1991; see Fig. 1). In type I, the package crack originates from the die pad/molding compound interface delamination. In type II, the package crack originates from the die attach/die pad interface

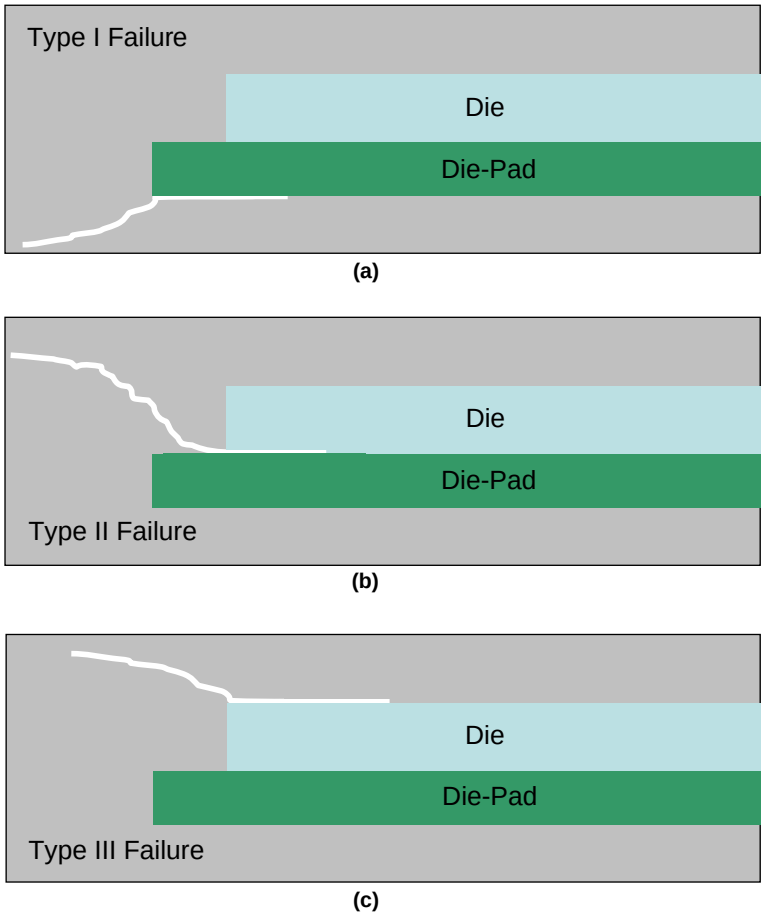

Fig. 1. Schematic of three types of package cracks. (a) Type I; (b) Type II; (c) Type III.

delamination. Type III refers to package crack originating from the die surface/mold compound interface delamination. Of the three, type II package cracking is least reported and understood. This study aims to gain some understanding of type II cracking, with particular attention to vapor pressure and residual stress effects on die attach failure.

Computational studies of interface delamination and failure taking account of vapor pressure effects were made by Cheng and Guo (2003) and Chong et al. (2004). They showed that vapor pressure effects are manifested in several ways: high vapor pressure within cavities accelerates void growth and coalescence; vapor pressure exerts tractions on the crack faces as well as shifts interface mode mixity from shear-dominated to tensile-dominated stress fields; vapor–pressure induced crack driving force is an increasing function of the crack size. Acting simultaneously, they cause interface delamination and failure exhibiting brittle-like characteristics which lead to popcorn cracking.

This paper continues the study begun by Guo and Cheng (2003). Using the centerline crack model of Varias et al. (1991), they investigated vapor pressure effects on failure of polymeric adhesives. The study described the interplay between stress elevation induced by constrained plastic flow and stress relaxation associated with vapor pressure assisted void growth and coalescence. Voiding activity takes place through three competing failure mechanisms: near-tip void growth and coalescence with the crack; void growth with formation of an extended damage zone emanating from the crack; and rapid void growth at large distances ahead of the crack leading to formation of multiple damaged zones. In their work, Guo and Cheng used a "partially porous adhesive" model wherein damage was confined to a well-delineated zone in the adhesive, viz. a single row of void-containing cells deployed directly ahead of the crack. Some background to the model can be found in Xia and Shih (1995).

Typical polymeric adhesives contain numerous pores and cavities (e.g. Trigg, 2003). This suggests that the whole polymeric adhesive could be treated as a porous material for purposes of studying damage arising from void growth and coalescence. Moreover, related studies showed that crack growth can occur at the crack front or along film/substrate interfaces (e.g. Chowdhury and Narasimhan, 1995, 2000a). Thus it appears that competition between different failure mechanisms could not be addressed by the partially porous adhesive model used in previous studies. Guided by these observations, the present study makes use of a "fully porous adhesive" model where pre-existing voids are distributed throughout the adhesive. Using this model, we investigate how adhesive porosity, vapor pressure and residual stress affect the outcome among competing failure mechanisms. The porous adhesive is described by an extended Gurson model incorporating vapor pressure effects (Guo and Cheng, 2001, 2002; Cheng and Guo, 2003).

2. Problem formulation

This work addresses symmetrically loaded joints. The adhesive contains a centerline crack which is long compared to the thickness of the adhesive as well as the extent of the plastic zone that develops in the adhesive. Under these conditions, the asymptotic problem shown in Fig. 2 is applicable. The centerline crack is taken to be semi-infinite and is loaded remotely by the symmetric Mode I K-field.

2.1. Material model

Around the glass transition temperature, T_g, certain polymers including epoxies behave like elastic–plastic solids exhibiting extensive ductility and hardening. Above T_g, large viscoelastic or viscoplastic deformations are possible (Gibson and Ashby, 1997, Chapter 3). Steenbrink et al. (1997) investigated void growth in glassy polymers that exhibit intrinsic softening and progressive strain hardening at large strains. Li and Pan (1990a,b) and Dong and Pan (1991) showed how pressure sensitivity affects hydrostatic stress levels ahead of the crack as well as the plastic zone size and shape in polymeric materials. Chowdhury and

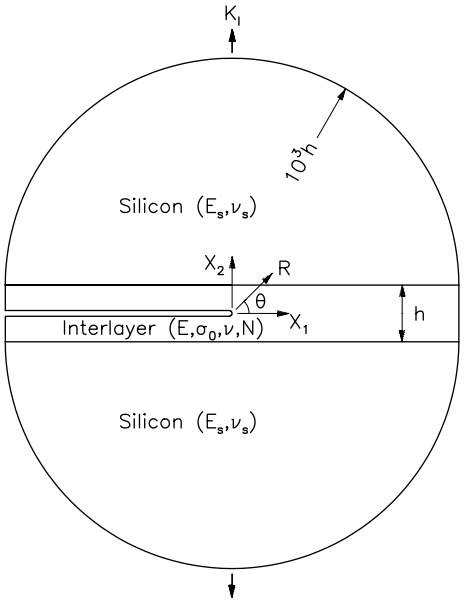

Fig. 2. An adhesive (with a centerline crack) bonded to two elastic substrates subject to remote elastic K_I field.

Narasimhan (2000a,b) found that the degree of pressure sensitivity could change the stress and deformation fields in a polymeric adhesive. They also showed that the fracture toughness of polymeric adhesives is enhanced as the degree of pressure sensitivity increases. A study of porous plastic solids exhibiting pressure sensitivity is in progress. In the present work, we assume that the adhesive at reflow conditions can be described as a rate-independent elastic power-law hardening material.

The joint comprises a ductile adhesive of thickness h joining two elastic substrates. The two substrates have identical properties. They are elastic isotropic materials with Young's modulus, E_s, and Poisson's ratio, ν_s.

The adhesive is elastically isotropic with Young's modulus E and Poisson's ratio ν. The plastic response of the adhesive is characterized by a J_2 flow theory (isotropic hardening based on Mises yield condition). The uniaxial tensile stress–strain behavior of the adhesive is described by a true stress–logarithmic strain relation

$$\begin{aligned} \varepsilon &= \frac{\sigma}{E}, && \sigma < \sigma_0, \\ \varepsilon &= \frac{\sigma_0}{E}\left(\frac{\sigma}{\sigma_0}\right)^{1/N}, && \sigma \geqslant \sigma_0, \end{aligned} \tag{1}$$

where σ_0 is the initial yield stress in tension, and N the strain hardening exponent.

Voids are distributed throughout the adhesive. To this end, the adhesive is modeled by several rows of void-containing cell elements. The behavior of the cell elements is described by the Gurson flow potential Φ (Gurson, 1977; Tvergaard, 1990) extended to take account of vapor pressure p (Guo and Cheng, 2002). It has the form:

$$\Phi = \left(\frac{\sigma_e}{\sigma_M}\right)^2 + 2q_1 f \cosh\left(\frac{3q_2(\sigma_m + p)}{2\sigma_M}\right) - \left[1 + (q_1 f)^2\right] = 0, \tag{2}$$

where σ_e denotes the equivalent macroscopic stress, σ_m the mean macroscopic stress and σ_M the flow stress of the matrix as determined by Eq. (1).

The vapor pressure, p, is a new internal variable given by

$$\frac{p}{p_0} = \frac{T}{T_0}\frac{f_0}{f}\frac{1-f}{1-f_0}\mathrm{e}^{-3\alpha\Delta T}, \tag{3}$$

which relates the current state (p,f,T) to the initial state (p_0,f_0,T_0). In the above, α is the coefficient of thermal expansion (CTE), ΔT is the temperature rise relative to the reference temperature T_0, and f is the current void volume fraction which obeys the volumetric plastic strain rate relation

$$\dot{f} = (1-f)\mathrm{tr}\,\mathbf{d}^{\mathrm{P}}. \tag{4}$$

In our isothermal analysis, we take $\Delta T = 0$. The micromechanics parameters q_1 and q_2 were introduced by Tvergaard (1990) to improve model predictions for periodic arrays of cylindrical and spherical voids, and are taken to be 1.25 and 1 respectively (Faleskog et al., 1998).

The initial residual stress σ_{R} in the ductile adhesive is prescribed by imposing the components of initial strain

$$\varepsilon_{11} = \varepsilon_{33} = -\frac{1-v}{E}\sigma_{\mathrm{R}}, \quad \varepsilon_{22} = \frac{2v}{E}\sigma_{\mathrm{R}} \tag{5}$$

in the film. This induces an in-plane, equi-biaxial residual stress

$$\sigma_{11} = \sigma_{33} = \sigma_{\mathrm{R}}, \quad \sigma_{22} = 0. \tag{6}$$

This modeling is supported by WARP3D (Gullerud et al., 2002) which provides the capability to define anisotropic thermal expansion coefficients for each element in the model. When the imposed element temperatures are unity, the expansion coefficients correspond to the initial strains applied at the onset of the analysis.

2.2. Boundary value problem

Fig. 3 displays the finite element model. By exploiting the symmetry of the crack geometry and the loading, we model only the upper half of the geometry shown in Fig. 2. The adhesive thickness h is equal to $8D$. Along the remote circular boundary, $R = 1000h$, the elastic asymptotic Mode I in-plane displacement fields

$$\begin{aligned} u_1(R,\theta) &= K_{\mathrm{I}}\frac{1+v_{\mathrm{s}}}{E_{\mathrm{s}}}\sqrt{\frac{R}{2\pi}}(3-4v_{\mathrm{s}}-\cos\theta)\cos\frac{\theta}{2}, \\ u_2(R,\theta) &= K_{\mathrm{I}}\frac{1+v_{\mathrm{s}}}{E_{\mathrm{s}}}\sqrt{\frac{R}{2\pi}}(3-4v_{\mathrm{s}}-\cos\theta)\sin\frac{\theta}{2} \end{aligned} \tag{7}$$

are prescribed. Here $R^2 = X_1^2 + X_2^2$ and $\theta = \tan^{-1}(X_2/X_1)$ for points on the remote boundary. Edge loads at the ends of the ductile adhesive are neglected since the error introduced is small (Tvergaard and Hutchinson, 1996).

The computations are carried out using a three-dimensional finite element program WARP3D (Gullerud et al., 2002). The finite element computational model consists of 2257 three-dimensional, 8-node linear elements (two-dimensional plane strain elements are not included in the element library offered by WARP3D). Plane strain conditions are achieved by prescribing out-of-plane displacements on all the nodes to vanish. The upper half of the adhesive is modeled by eight rows of void-containing cell elements, each of dimension $D/2$ by $D/2$ (see Fig. 3c). Each cell element has a void of initial volume fraction f_0 associated with initial vapor pressure p_0. Hereafter, this computational model is referred to as the fully porous adhesive (FPA) model.

For comparison purposes, computations were also performed in which void growth is confined to a narrow zone directly ahead of the crack. In this case, only one row of void-containing cell elements, each

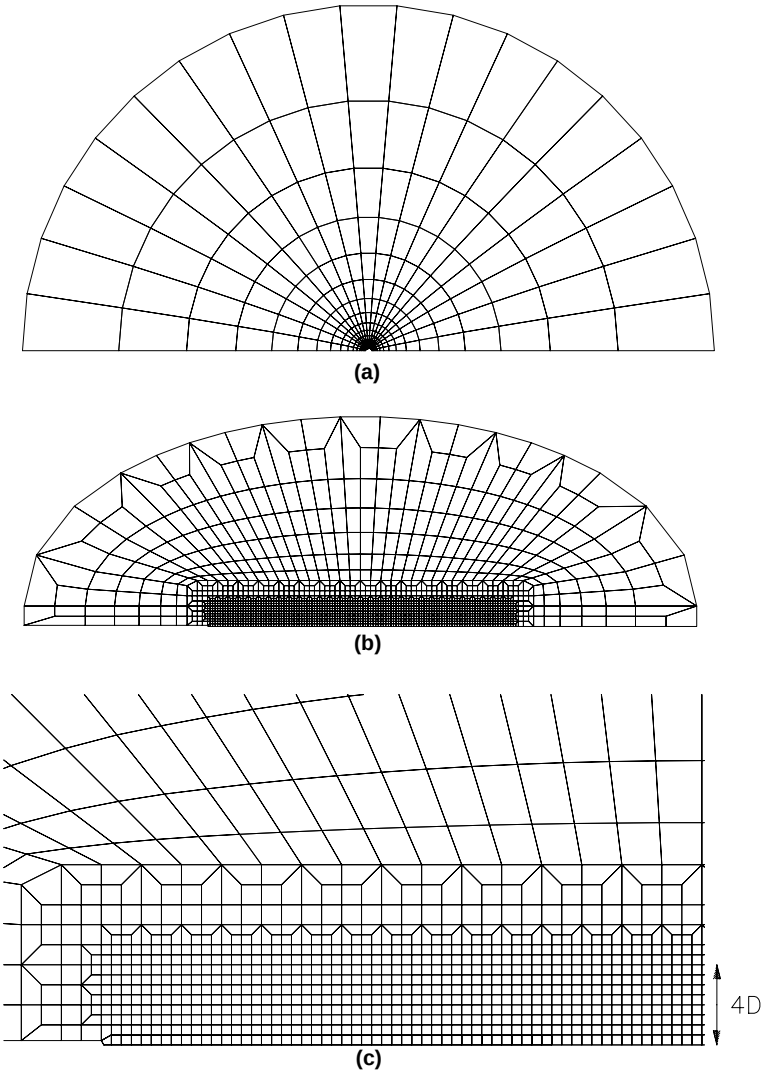

Fig. 3. Finite element mesh for small scale yielding analysis. (a) Mesh of outer region. (b) Refined mesh of inner region. (c) Near-tip mesh with several layers of void-containing cell elements ($D/2$ by $D/2$). Cell is characterized by f_0 and p_0.

of dimension $D/2$ by $D/2$, is deployed ahead of the crack. This partially porous adhesive (PPA) model is similar to the geometric models employed by Guo and Cheng (2003) for damage evolution simulations and by Xia and Shih (1995) for crack growth studies. The void-free adhesive material is described by (1).

For the crack geometry depicted in Fig. 2, Irwin's relation between the stress intensity factor K_I and the energy release rate G for a plane strain crack in an elastic solid is

$$G = \frac{1-\nu_s^2}{E_s} K_I^2. \tag{8}$$

Small-scale yielding conditions prevail when the plastic zone size in the adhesive is small compared to the distance to the remote boundary R. In this case, the J-integral can be interpreted as the remote/applied energy release rate G. At various stages of loading, the value of the J-integral is calculated on a number of

contours around the crack using the domain integral method (Moran and Shih, 1987). The domain integral value is found to be in good agreement with the value given by (8). This consistency check assures that small-scale yielding conditions are satisfied.

3. Results and discussion

From dimensional considerations, the spatial distribution of field quantities σ_m/σ_0 and f depends on the following dimensionless geometric-material parameters:

$$\frac{J}{\sigma_0 h}, \frac{h}{D}; \quad \frac{\sigma_0}{E}, \frac{E_s}{E}, N, \nu, \nu_s; \quad f_0, \frac{p_0}{\sigma_0}, \frac{\sigma_R}{\sigma_0}. \tag{9}$$

The properties of the elastic–plastic adhesive are specified by the parameters $\sigma_0/E = 0.01$, $\nu = 0.4$, and $N = 0.1$. A typical level of elastic modulus mismatch between the adhesive and the substrate considered is $E_s/E = 10$, with $\nu_s = 0.3$. In this study, we direct attention to the process related parameters below:

$$f_0, \frac{p_0}{\sigma_0}, \frac{\sigma_R}{\sigma_0}. \tag{10}$$

Estimates of f_0 for typical adhesives and molding compounds, based on moisture analyses, range from 1% to 5% (Galloway and Miles, 1997). Studies by Liu and Mei (1995) suggest that vapor pressures can reach 3–6 MPa during the reflow process. Such levels are comparable to the yield stresses of adhesives and molding compounds at T_g (Gibson and Ashby, 1997). Other studies indicate that the thermal expansion mismatch between the adhesive and the die can generate stresses exceeding the yield strength of the adhesive (Evans and Hutchinson, 1995; Tvergaard and Hutchinson, 1996).

Guided by the above, initial porosities f_0 of 1% and 5%, initial vapor pressure $p_0 = \sigma_0$, and residual stress $\sigma_R = \sigma_0$ will be considered in the present work. In most of the cases reported here voiding develops primarily in the zone directly ahead of the crack. For such cases, the mean stress and void volume fraction distributions along the midplane of the adhesive layer (at $X_2 = 0$) are displayed. When voiding occurs near the adhesive/substrate interface, the fields along the interface (at $X_2 = 0.5h$) are shown.

3.1. Failures of low and high porosity adhesives

Sources that contribute to the initial porosity of an adhesive include the pre-existing pores/cavities in the adhesive and filler particles that are weakly bonded to the polymeric matrix. We begin by presenting results for the fully porous adhesive (FPA).

Fig. 4a displays the evolution of f for a low porosity adhesive, $f_0 = 0.01$, under pure remote loading. At applied load of $J/(\sigma_0 h) = 0.082$, the solid line labeled 0.082 shows voids adjacent to the crack tip growing rapidly with near-tip f reaching about 0.1. At the same time, a second and smaller peak ($f = 0.03$) in void activity can be found at distance $X_1 = 1.5h$ ahead of the crack. When the load is increased slightly to $J/(\sigma_0 h) = 0.089$, there is a sudden burst in void activity. Voids in the vicinity of $X_1 = 1.5h$ grow rapidly to levels well beyond $f = 0.1$. At even higher loadings not shown here, the highly damaged zone centered about $X_1 = 1.5h$ joins with the crack front. Concurrently, new zones of voiding are formed even further ahead of the crack.

To provide a more complete picture of the above sequence of void activity, we examine the stress profiles corresponding to $J/(\sigma_0 h) = 0.082$, and 0.089 shown in Fig. 4b. The solid line labeled 0.082 shows the build up of the mean stress associated with constrained plastic flow. At a higher load level of $J/(\sigma_0 h) = 0.089$, stresses in vicinity of $X_1 = 1.5h$ fall sharply. The stress relaxation, extending over a spatial interval of about $2h$, is associated with rapid void growth centered about $X_1 = 1.5h$ shown in Fig. 4a. The solid lines in Fig. 4a and b depict the interplay between stress elevation induced by constrained plastic flow and stress

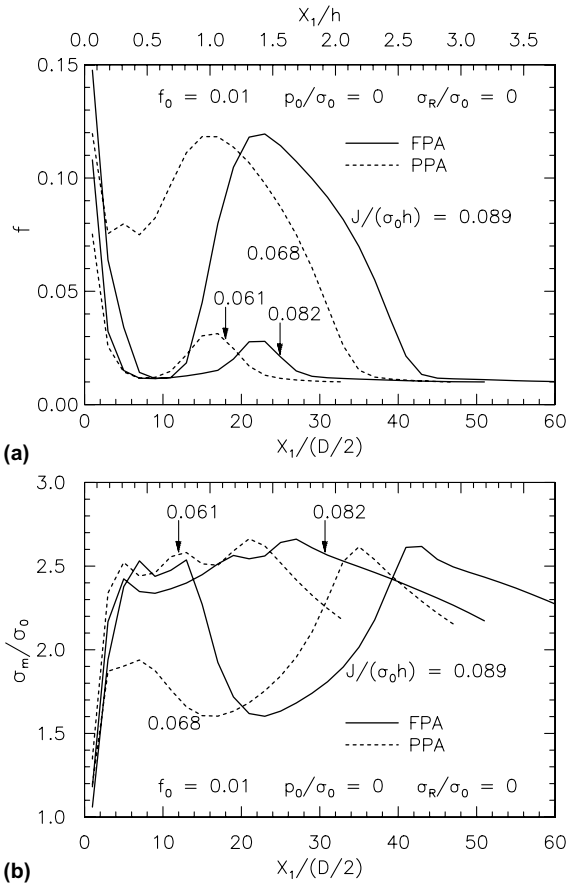

Fig. 4. Porosity f and mean stress σ_m/σ_0 ahead of crack ($X_2 = 0$); $f_0 = 0.01$, remote load only.

relaxation associated with extensive void growth. The figure also shows that voiding occurs in a particular sequence—voiding begins near the crack tip followed by accelerated void growth at large distances ahead of the crack. This voiding pattern is referred to as "multiple damage zone" mechanism.

At this juncture, we make contact with work by Guo and Cheng's (2003) on adhesive failure. The porosity distribution shown by the dashed curves in Fig. 4a and b are obtained using the partially porous adhesive (PPA) model. It is noteworthy that the sequence of voiding and its patterns (dashed lines) for the PPA are similar to those for the FPA (solid lines). However, at comparable load levels, the PPA model overestimates the damage ahead of the crack.

Fig. 5 presents results for a high porosity adhesive, $f_0 = 0.05$. Results for the FPA are taken up first. A zone of voiding emanates from the crack at low load—see solid curve labeled by 0.044 in Fig. 5a. The corresponding stress distribution is shown in Fig. 5b—see solid curve labeled by 0.044. As the load increases, voids further ahead of the crack also grow by significant amounts—see solid curve labeled by 0.066. The stress relaxation associated with this pattern of voiding shifts the peak stress location further ahead of the crack—from $X_1 = 0.5h$ to $X_1 = 3h$. The distance between the peak stress location and the crack tip demarcates the physical extent of the damage zone. At $J/(\sigma_0 h) = 0.066$, the damage zone extends over a distance $3h$ ahead of the crack. This pattern of adhesive failure is referred to as "contiguous damage zone" mechanism.

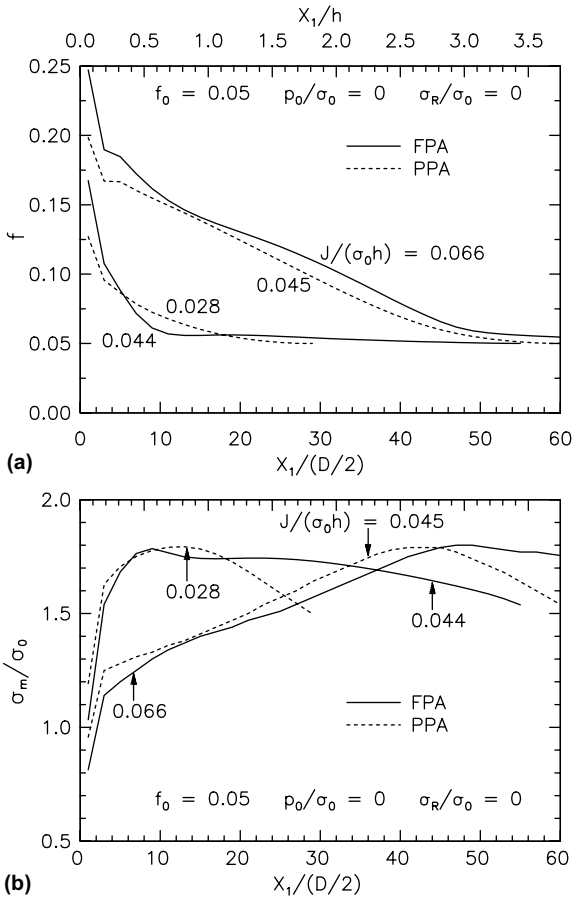

Fig. 5. Porosity f and mean stress σ_m/σ_0 ahead of crack ($X_2 = 0$); $f_0 = 0.05$, remote load only.

Void growth and stress distributions predicted by the PPA model are shown by dashed lines in Fig. 5. While the pattern of voiding is similar to that for the FPA model, the PPA model overestimates damage levels directly ahead of the crack.

The porosity profiles in Figs. 4 and 5 reveal a crucial character of adhesive damage. The damage zone size is a non-linear function of the applied load—a small load increment can cause a disproportionately large increase in the damage zone size. For example, a 50% increase in the load (from 0.044 to 0.066) produces a sixfold increase in the size of the damage zone (from 0.5h to 3h, see Fig. 5).

3.2. Temperature/moisture effects on failures of low porosity adhesives

Vapor pressure and residual stress effects on damage in low porosity adhesives are taken up here. High residual stresses, comparable to the adhesive's yield strength, are not uncommon in IC packages where adhesives are deposited at elevated temperatures. Evans and Hutchinson (1995), Huang et al. (1996) and Guo and Cheng (2001) have discussed residual stress effects on voiding and interface cracking. Tvergaard and Hutchinson (1996) showed that residual tensile stresses in a ductile adhesive can lower the joint toughness significantly.

Moisture resides in pores and cavities of adhesives as well as at adhesive/particle and adhesive/die interfaces. During the reflow soldering process, the condensed moisture vaporizes. The rapidly expanding water vapor generates internal pressures (on the voids) that can reach 3–6 MPa. These levels are comparable to the yield strengths of the adhesives when the reflow soldering temperature exceeds the adhesive's T_g. Chew et al. (2004) have studied the combined effect of vapor pressure and residual stress on joint toughness.

We begin by presenting the results for a low porosity adhesive, $f_0 = 0.01$. The stress arising from thermal expansion mismatch between the adhesive and the substrate is treated as an initial residual tensile stress of magnitude $\sigma_R = \sigma_0$. Rapid vaporization of moisture at high temperature introduces an initial vapor pressure on the void of magnitude $p_0 = \sigma_0$.

Fig. 6a displays the damage distribution, at $J/(\sigma_0 h) = 0.060$, under four types of loading: (i) remote load only; (ii) remote load with vapor pressure ($p_0 = \sigma_0$); (iii) remote load with residual stress ($\sigma_R = \sigma_0$); (iv) remote load with vapor pressure and residual stress ($p_0 = \sigma_R = \sigma_0$). With the exception of loading type (iii), damage by void growth under the other three load types is concentrated in the zone directly ahead of the crack.

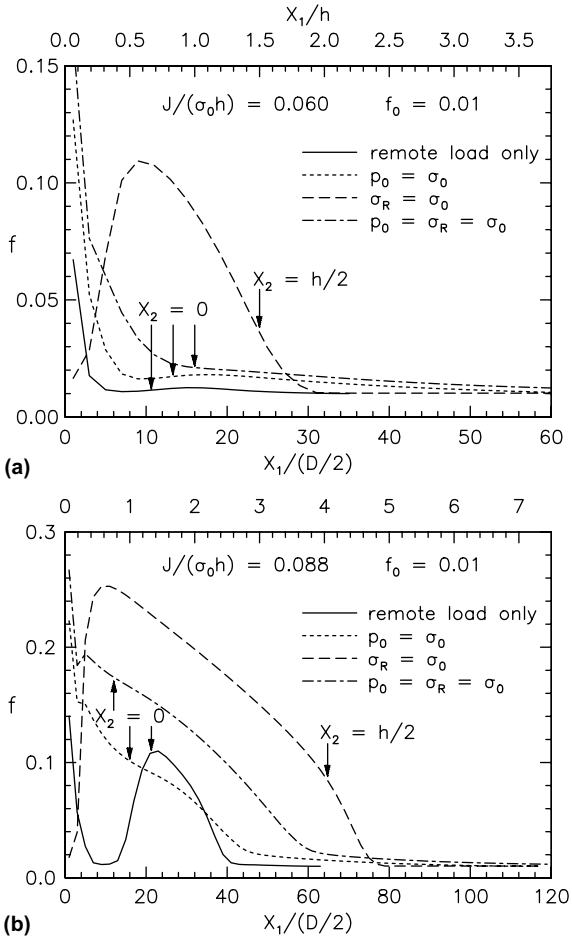

Fig. 6. Porosity f ahead of crack ($X_2 = 0$) and along adhesive/substrate interface ($X_2 = 0.5h$) under four types of loading. $f_0 = 0.01$, (i) remote load only; (ii) $p_0 = \sigma_0$, $\sigma_R = 0$; (iii) $\sigma_R = \sigma_0$, $p_0 = 0$; (iv) $p_0 = \sigma_R = \sigma_0$.

Fig. 6b shows the damage distribution at $J/(\sigma_0 h) = 0.088$. As noted in the previous section in connection with Fig. 4, the multiple damage zone mechanism prevails under load type (i). Contiguous damage zones are formed under load types (ii) and (iv).

Under load type (iii), voids near the mid-plane ($X_2 = 0$) experienced relatively little growth whereas voids at the adhesive/substrate interface grow rapidly. The dash lines in Fig. 6a and b depict the progression of voiding at the adhesive/substrate interface ($X_2 = 0.5h$).

Fig. 7 displays contour maps of void activity associated with load types (i)–(iv). Three distinctive damage patterns can be seen. The topmost plot displays contours of $f = 0.05$ under load type (i). At $J/(\sigma_0 h) = 0.070$ voiding occurs near the tip. At $J/(\sigma_0 h) = 0.088$, intense voiding activity develops far ahead of the crack with the new damage zone being centered about $X_1 = 1.5h$ (compare with profile of solid line in Fig. 6b). At even

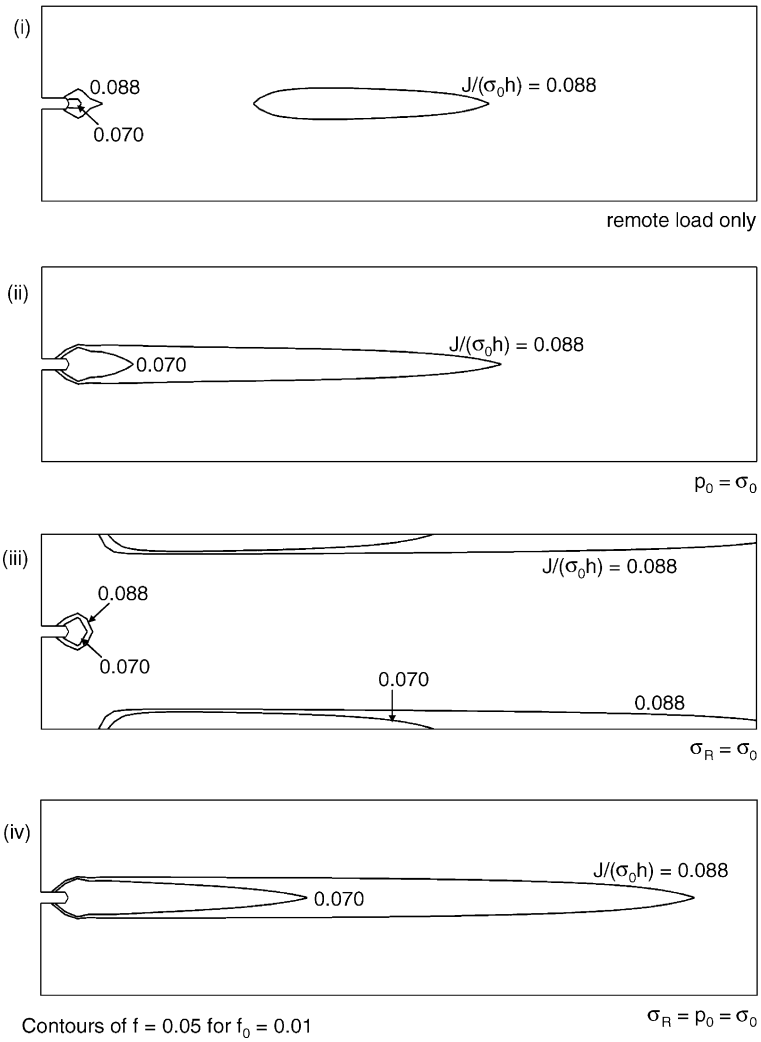

Fig. 7. Contours of $f = 0.05$ for $J/(\sigma_0 h) = 0.070$ and $J/(\sigma_0 h) = 0.088$ under four types of loading. $f_0 = 0.01$, (i) remote load only; (ii) $p_0 = \sigma_0$, $\sigma_R = 0$; (iii) $\sigma_R = \sigma_0$, $p_0 = 0$; (iv) $p_0 = \sigma_R = \sigma_0$.

higher loads, additional zones of void activity form even further ahead of the crack. This pattern of voiding has been referred to as multiple damage zone mechanism.

The second and fourth plots show extended damage zones emanating from the crack at $J/(\sigma_0 h) = 0.070$ and 0.088. The voiding pattern that develops under load type (ii) and (iv) belong to the contiguous damage zone mechanism.

The third plot shows void growth occurring near the crack tip as well as along the adhesive/substrate interfaces under load type (iii). At both load levels, $J/(\sigma_0 h) = 0.070$ and 0.088, voiding occurs primarily along the adhesive–substrate interface with peak porosities developing at about 45° to the initial crack tip.

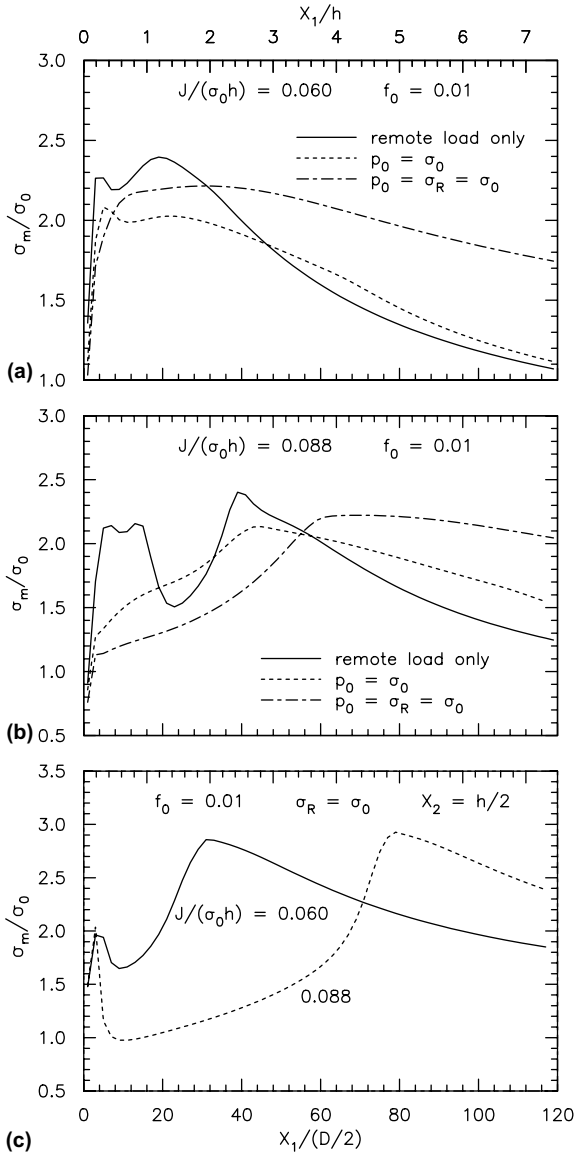

Fig. 8. Mean stress under four types of loading for $f_0 = 0.01$. (a) and (b) Stress ahead of crack ($X_2 = 0$); (i) remote load only; (ii) $p_0 = \sigma_0$, $\sigma_R = 0$; (iv) $p_0 = \sigma_R = \sigma_0$. (c) Stress along adhesive/substrate interface ($X_2 = 0.5h$); (iii) $\sigma_R = \sigma_0$, $p_0 = 0$.

The centerline crack offers a model problem to study fracture under constrained plastic flow. A change in the initial crack-tip configuration would affect the evolution of stress triaxiality which in turn influences the mechanisms of damage. The implications of this geometrical effect will be discussed in a future study.

It is noteworthy that the four plots in Fig. 7 display a common trend. A small load increase induces a disproportionately large increase in the size of the damage zone. In other words, small load variations with time can cause rapid damage propagation. This behavior could explain the catastrophic nature of popcorn cracking.

Stress distributions ahead of the crack ($X_2 = 0$) associated with load types (i), (ii) and (iv) at load levels $J/(\sigma_0 h) = 0.060$ and 0.088, are displayed in Fig. 8a and b respectively. Fig. 8c shows the stresses at the interface ($X_2 = 0.5h$) under load type (iii). The patterns of stress elevation/relaxation displayed in Fig. 8 are consistent with the voiding patterns shown in Figs. 6 and 7.

3.3. Temperature/moisture effects on failures of high porosity adhesives

We present results for a high porosity adhesive, $f_0 = 0.05$, in this section. Fig. 9a and b display the voiding profiles at $J/(\sigma_0 h) = 0.050$ and 0.070, respectively. Voiding activity, under all four load types, is concen-

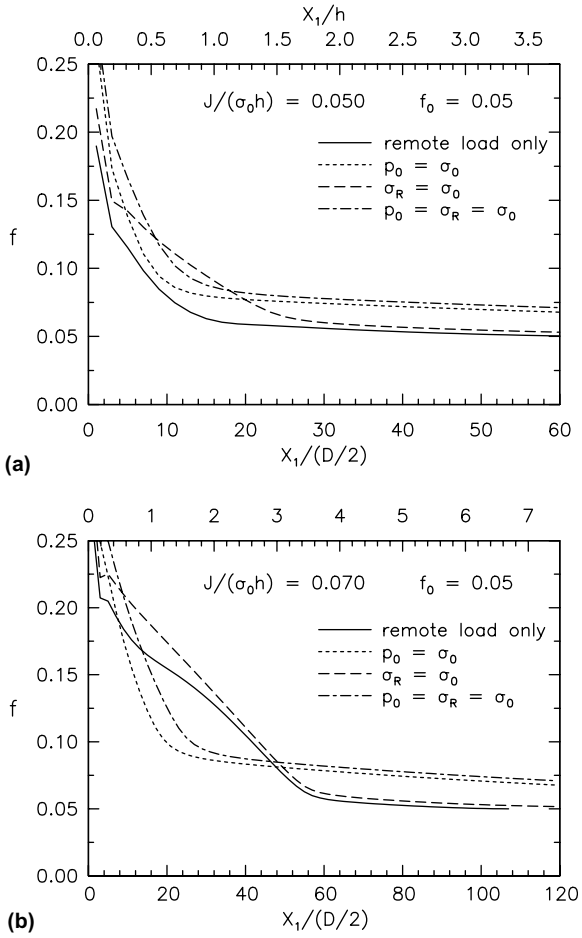

Fig. 9. Porosity f ahead of crack ($X_2 = 0$) under four types of loading. $f_0 = 0.05$, (i) remote load only; (ii) $p_0 = \sigma_0$, $\sigma_R = 0$; (iii) $\sigma_R = \sigma_0$, $p_0 = 0$; (iv) $p_0 = \sigma_R = \sigma_0$.

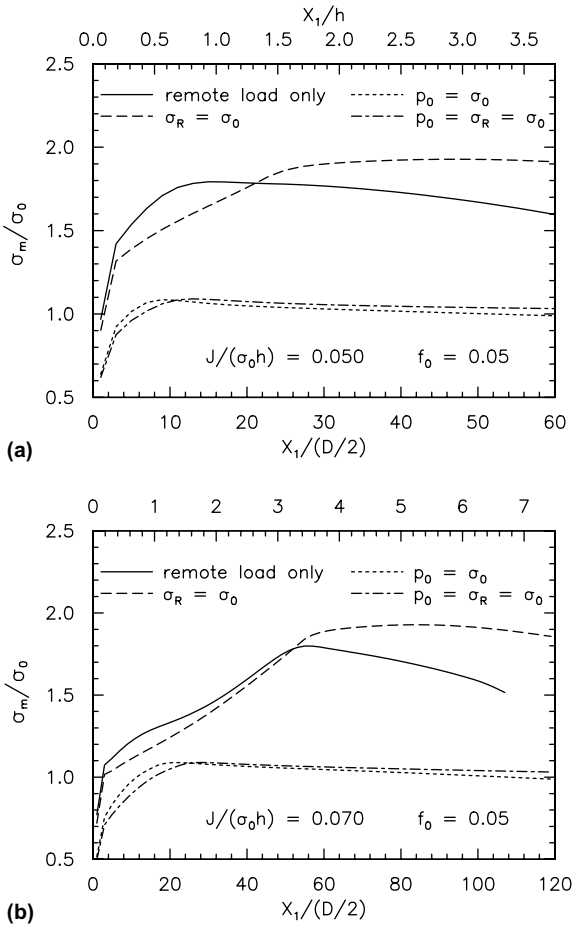

Fig. 10. Mean stress ahead of crack ($X_2 = 0$) under four types of loading. $f_0 = 0.05$, (i) remote load only; (ii) $p_0 = \sigma_0$, $\sigma_R = 0$; (iii) $\sigma_R = \sigma_0$, $p_0 = 0$; (iv) $p_0 = \sigma_R = \sigma_0$.

trated in the zone directly ahead of the crack. The pattern of voiding belongs to the contiguous damage zone mechanism.

Fig. 10 shows stress elevation/relaxation under the four load types. The stress distributions for load types (i) and (iii) display the elevation/relaxation characteristics seen in Figs. 5 and 8. By contrast stress distributions, associated with load types (ii) and (iv), over the entire damage zone are relatively uniform. This suggests that stress relaxation is balanced by stress elevation—a behavior that appears to be peculiar to high porosity adhesive subjected to high vapor pressure.

4. Concluding remarks

This work is aimed at understanding die attach failure during reflow soldering, commonly referred to as a type II failure, and how it could lead to popcorn cracking. With this in mind, the computational study is focused on a ductile polymeric adhesive joining two elastic substrates paying particular attention to failure mechanisms which are precursors to popcorn cracking. We observe that ductile polymeric adhesives can fail

by one of three damage mechanisms: (i) contiguous damage zone emanating from the crack; (ii) multiple damage zones forming at distances of several adhesive thicknesses ahead of the crack; and (iii) extensive damage zone advancing along the adhesive/substrate interfaces. Our results show a common character—the damage zone size is a non-linear function of the applied load. That is, a small increase in load can induce a disproportionately large increase in the size of the damage zone. Experimental studies on type II package cracking have shown that plastic packages could fail by interface delamination and/or rupture of the die-attach layer (e.g. Alpern et al., 2002; Tay and Lin, 1999; Pang and Seetoh, 1997; Pang et al., 2002). The numerically simulated behaviors are consistent with these experimentally observed failure mechanisms.

The multiple damage zone mechanism is operative in low porosity adhesives, while a rapidly advancing contiguous damage zone emanating from the main crack is found in high porosity adhesives. The latter mechanism is also favored when the voids are subjected to high vapor pressure. In low porosity adhesives, residual stress enhances damage near the adhesive/substrate interface.

Our computational results indicate that residual tensile stress and in particular vapor pressure accelerate voiding activity as well as the growth of the damage zone. This behavior offers an explanation for the catastrophic nature of popcorn cracking. In low porosity adhesives, $f_0 = 0.01$, residual stress effects dominate over vapor pressure effects. In high porosity adhesives, $f_0 = 0.05$, vapor pressure effects are dominant. The operative mechanism appears to depend on the porosity level of the adhesive as well as the relative proportion of remote load to residual stress and vapor pressure.

The fully porous adhesive model used in this study appears capable of simulating all three failure mechanisms noted above under a wide range of conditions. With one important exception, the partially porous adhesive model correctly predicts voiding and stress patterns in both low and high porosity adhesives. However it generally overestimates the damage level ahead of the crack. We should point out that porosity distributions in typical adhesives are likely to be non-uniform. In this regard, the FPA and the PPA models can be viewed as two limits of a large set of possible non-uniform initial porosity distributions. A study of failure mechanisms in adhesives with non-uniform initial porosity distribution is in progress.

Acknowledgments

The support of this work by the National University of Singapore (Grant no. R-265-000-136-112) is gratefully acknowledged.

References

Alpern, P., Dudek, R., Schmidt, R., Wicher, V., Tilgner, R., 2002. On the mode II popcorn effect in thin packages. IEEE Transactions on Components and Packaging Technologies 25 (1), 56–65.

Cheng, L., Guo, T.F., 2003. Vapor pressure assisted void growth and cracking of polymeric films and interfaces. Interface Science 11, 277–290.

Chew, H.B., Guo, T.F., Cheng, L., 2004. Vapor pressure and residual stress effects on the toughness of polymeric adhesive joints. Engineering Fracture Mechanics 71, 2435–2448.

Chong, C.W., Guo, T.F., Cheng, L., 2004. Vapor pressure assisted crack growth at interfaces under mixed mode loading. Computational Materials Science 30, 425–432.

Chowdhury, R.S., Narasimhan, R., 1995. Finite element simulations of ductile rupture in a constrained metal foil. Material Science and Engineering A 191, 27–37.

Chowdhury, R.S., Narasimhan, R., 2000a. A finite element analysis of stationary crack tip fields in a pressure sensitive constrained ductile layer. International Journal of Solids and Structures 37, 3079–3100.

Chowdhury, R.S., Narasimhan, R., 2000b. A finite element analysis of quasistatic crack growth in a pressure sensitive constrained ductile layer. Engineering Fracture Mechanics 66, 551–571.

Dong, P., Pan, J., 1991. Elastic–plastic analysis of cracks in pressure sensitive materials. International Journal of Solids and Structures 28, 1113–1127.

Evans, A.G., Hutchinson, J.W., 1995. The thermomechanical integrity of thin films and multilayers. Acta Metallurgica et Materialia 43 (7), 2507–2530.

Faleskog, J., Gao, X., Shih, C.F., 1998. Cell model for non-linear fracture analysis—I. Micromechanics calibration. International Journal of Fracture 89, 355–373.

Fukuzawa, I., Ishiguro, S., Nanbu, S., 1985. Moisture resistance degradation of plastic LSIs by reflow soldering. In: IEEE/IRPS International Reliability of Physics Symposium, pp. 192–197.

Galloway, J.E., Miles, B.M., 1997. Moisture absorption and desorption predictions for plastic ball grid array packages. IEEE Transactions on Components Packaging and Manufacturing Technology Part A 20 (3), 274–279.

Gibson, L.J., Ashby, M.F., 1997. Cellular Solids: Structure and Properties, second ed. Cambridge University Press, Cambridge, UK.

Gullerud, A.S., Koppenhoefer, K.C., Ruggieri, C., Dodds, Jr. R.H., 2002. WARP3D: 3-D dynamic nonlinear fracture analysis of solids using parallel computers and workstations. Civil Engineering Studies, Structural Research Series No. 607, UILU-ENG-95-2012, University of Illinois at Urbrana-Champaign.

Guo, T.F., Cheng, L., 2001. Thermal and vapor pressure effects on cavitation and void growth. Journal of Materials Science 36 (24), 5871–5879.

Guo, T.F., Cheng, L., 2002. Modeling vapor pressure effects on void rupture and crack growth resistance. Acta Materialia 50 (13), 3487–3500.

Guo, T.F., Cheng, L., 2003. Vapor pressure and void size effects on failure of a constrained ductile film. Journal of the Mechanics and Physics of Solids 51, 993–1014.

Gurson, A.L., 1977. Continuum theory of ductile rupture by void nucleation and growth: Part I—Yield criteria and flow rules for porous ductile media. Journal of Engineering Materials and Technology 99, 2–15.

Huang, Y., Hu, K.X., Yeh, C.P., Li, N.Y., Hwang, K.C., 1996. A model study of thermal stress-induced voiding in electronic packages. Journal of Electronic Packaging 118, 229–234.

Li, F.Z., Pan, J., 1990a. Plane-strain crack-tip fields for pressure-sensitive dilatant materials. Journal of Applied Mechanics 57, 40–49.

Li, F.Z., Pan, J., 1990b. Plane-stress crack-tip fields for pressure-sensitive dilatant materials. Engineering Fracture Mechanics 35, 1105–1116.

Liu, S., Mei, Y., 1995. Behavior of delaminated plastic IC packages subjected to encapsulation cooling, moisture absorption, and wave soldering. IEEE Transactions on Components Packaging and Manufacturing Technology Part A 18 (3), 634–645.

Moran, B., Shih, C.F., 1987. A general treatment of crack tip contour integrals. International Journal of Fracture 35, 363–371.

Omi, S., Fujita, K., Tsuda, T., Maeda, T., 1991. Causes of cracks in SMD and type-specific remedies. IEEE Transactions on Components Packaging and Manufacturing Technology 14 (4), 818–823.

Pang, H.L.J., Seetoh, C.W., 1997. A compact mixed mode (CMM) fracture specimen for adhesive bonded joints. Engineering Fracture Mechanics 57, 57–65.

Pang, H.L.J., Zhang, X., Shi, X., Wang, Z.P., 2002. Interfacial fracture toughness test methodology for adhesive bonded joints. IEEE Transactions on Components and Packaging Technologies 25 (2), 187–191.

Steenbrink, A.C., Van der Giessen, E., Wu, P.D., 1997. Void growth in glassy polymers. Journal of the Mechanics and Physics of Solids 45, 405–437.

Tay, A.A.O., Lin, T.Y., 1999. Influence of temperature, humidity, and defect location on delamination in plastic IC packages. IEEE Transactions on Components and Packaging Technologies 22 (4), 512–518.

Trigg, A., 2003. Applications of infrared microscopy to IC and MEMs packaging. IEEE Transactions on Electronics Packaging Manufacturing 26 (3), 232–238.

Tvergaard, V., 1990. Material failure by void growth to coalescence. Advances in Applied Mechanics 27, 83–151.

Tvergaard, V., Hutchinson, J.W., 1996. On the toughness of ductile adhesive joints. Journal of the Mechanics and Physics of Solids 44 (5), 789–800.

Varias, A.G., Suo, Z., Shih, C.F., 1991. Ductile failure of a constrained metal foil. Journal of the Mechanics and Physics of Solids 39 (7), 963–986.

Xia, L., Shih, C.F., 1995. Ductile crack growth—I. A numerical study using computational cells with microstructurally based length scales. Journal of the Mechanics and Physics of Solids 43 (2), 233–259.